Measurement of Flow in a Microfluidic Channel in Response to Application of Voltage

By

Elizabeth A. Soukup

SUBMITTED TO THE DEPARTMENT OF MECHANICAL ENGINEERING IN PARTIAL FULFILLMENT OF THE REQUIREMENTS FOR THE DEGREE OF

BACHELOR OF SCIENCE IN MECHANICAL ENGINEERING
AT THE
MASSACHUSETTS INSTITUTE OF TECHNOLOGY

JUNE 2014

Signature of Author: Signature redacted

Department of Mechanical Engineering
May 19th, 2014

Certified by: Signature redacted

José Alvarado
Postdoctoral Associate
Thesis Supervisor

Accepted by: Signature redacted

Annette Hosoi
Associate Professor of Mechanical Engineering
Undergraduate Officer

Measurement of Flow in a Microfluidic Channel in Response to Application of Voltage

By

Elizabeth A. Soukup

Submitted to the Department of Mechanical Engineering on May 19th, 2014 in Partial Fulfillment of the Requirements for the Degree of Bachelor of Science in Mechanical Engineering

ABSTRACT

This thesis explores two methods of calculating the flow of Electrorheological fluid in a microfluidic channel in response to a gradient in an electric field: MATLAB simulation and microscopy experiments. Electrorheological fluid, which is composed of particles suspended in a liquid, has the property of changing its viscosity under the application of an electric field. The particles become polarized in an electric field, aligning themselves with a force that is proportional to the gradient of the electric field. The drag force equally opposes the dipole force and can entrain fluid and force it to move along the length of a channel. The dipole force was estimated using a MATLAB simulation, and the drag force was calculated via experiments which used Electrorheological fluid in a channel lined with electrodes. Although the two methods did not correlate in magnitude, they did agree in terms of general behavior, and net motion of fluid in a channel was achieved.

Thesis Supervisor: José Alvarado
Title: Postdoctoral Associate

Acknowledgements

This thesis would not have been possible without the consistent, kind, and informative guidance of Dr. José Alvarado, who taught me how to find meaning in a mess of data. Theresa Hoberg was also instrumental in helping me start the project and walking me through her simulation. Dr. Michael Evzelman, Dr. Matther Demers, and Dr. Anette Hosoi each contributed to my understanding of solid-state pumps and how the electrical and physical components work together. Ahmed Helal and Jean Comtet were very helpful in demonstrating proper use of the equipment required to successfully run these experiments.

Section 1: Introduction to Solid-State Pumps

1.1 Motivation and Principles

The need for microfluidic devices is large and multidisciplinary, ranging from applications in military transport to medicine. One example is Boston Dyanmic's BigDog- a rough-terrain load-carrying robot the size of a boar- which uses sixteen hydraulic actuators to control its extremely stable and self-righting chassis[1]. The 0.34m long LittleDog has three electric motors powering each of its four legs[2], which indicates a lag in the fluid technology required to power LittleDog in the same way of BigDog. Another, even smaller example is the self-powered blood analysis system that uses a mere 5μL of whole blood to separate components into red blood cells, white blood cells, and plasma[3].

The Reynolds number Re is a dimensionless ratio of inertia to viscosity that is frequently used to characterize fluid flow, and is very relevant to the construction of microfluidic systems. Defined as

$$Re = \frac{\rho v D}{\mu}, \tag{1}$$

where ρ is fluid density, v is flow velocity, D is the length scale, and μ is fluid velocity, Re can fall below 1 for very viscous fluids or fluids in small length scale systems (i.e. below 1 mm). Several notable differences exist between low (i.e. Re < 1) and high (i.e. Re > 1) Reynolds numbers flows, and this means that microfluidic systems behave very differently from larger fluid systems where Re > 1.

One particularly daunting challenge is the time-reversibility of low Re flows; as discussed in Purcell's *Life at Low Reynolds Number*, the Navier-Stokes equation for a small Reynolds number simplifies to contain zero time-dependent terms[4]. What this suggests for developing low Re systems is that a novel means of generating flow is required to have any net resulting motion. Additionally, the same losses that plague larger systems provide even greater difficulties in microfluidic devices, because the same tolerances for a system meters in size are comparatively much larger when the system shrinks by several orders of magnitude[5]. The compounding effect of these losses with standard mechanical and electrical losses in pumping devices result in efficiencies of 1% or less[6].

The goal of this thesis is to investigate a new alternative strategy known as the solid-state pump that will address the issues associated with microfluidic devices described above. The solid-state pump moves fluid through a system without any mechanical parts through the means of an electrorheological (ER) fluid, described in detail in section 1.2. When an ER fluid is exposed to an appropriate electric field, motion of the fluid occurs, and because there are no physical losses in the interface between the field and the fluid, the ultimate pump efficiency has the potential to be significantly higher.

Section 1.2 Electrorheological fluids

ER fluids are a non-naturally occurring substance consisting of solid particles suspended in a liquid substrate. As suggested by the name, the fluid flow properties change in response to an imposed electric field as the particles orient themselves and chain together[7]. The fluid, typically an oil, contains small ($\sim 10^{-6}$m diameter) dielectric particles. When a channel containing the fluid is exposed to an electric field, these dielectric particles polarize and reorient themselves along the direction of the field, forming chains that can span the width of the channel[8]. These particle chains can increase the viscosity of the fluid by several orders of magnitude from its non-energized state[9]. Current applications of ER fluid include variable damping control in systems with mechanical vibrations[10] and substance to measure force response in tactile displays[11].

Previous research has investigated the formation of particle chains resulting from the application of high voltages, which can be controlled to move fluid in a solid-state pump. In these experiments, a steady flow of ER fluid was introduced into a microfluidic channel[12]. Electric fields were generated perpendicular to the direction of the channel. Dense particle aggregation occurred in response to high voltage, particularly near the flow inlet where free particles were constantly being introduced.

There are two potential ways in which the properties of an ER fluid can lend themselves to being used in a solid-state pump. The first way has been briefly explained above: static, high voltage systems form particle chains which can be used as valves to block fluid in a channel. If a wave of high voltage is stepped across electrodes, this will cause motion of aggregated particle chains, forming a "moving wall" to push fluid along (figure 1). The other, less-understood way is the drag force of individual particle in ER fluid "pulling" the fluid along the length of the channel[13].

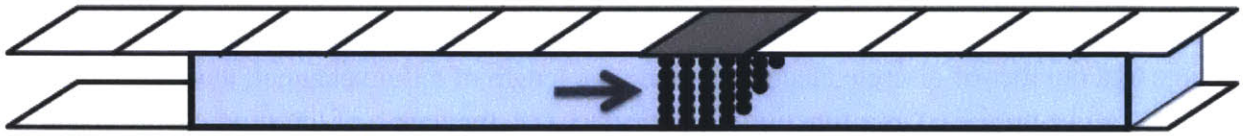

Figure 1: The walls of the channel are divided into discrete segments, each representing an electrode. High voltages, such as the one imposed on the grey electrode, cause particle aggregation into chains, represented by the black dots underneath the grey electrode. When voltage is manipulated such that high potentials translate in the direction of the arrow, fluid is pushed forward[14].

Section 1.3 A New Kind of Pump

This thesis aims to isolate the properties associated with the strategy of using particle drag force to stimulate flow in a microfluidic device. It is important to explain the dipole moment to understand how particle orientation produces net fluid movement. The dipole moment is a measure of the separation of positive and negative charges in a particle, and for uncharged particles, it quantifies how polarized they become in the presence of an electric field.

Mathematically, the dipole moment vector p is proportional to electric field strength E by a proportionality constant α

$$p = \alpha E \quad (2).$$

The force in the x-direction F_x associated with a dipole moment in an electric field in turn is

$$F_x = (p.\nabla)E = p_x \frac{\partial}{\partial x} E_x + p_y \frac{\partial}{\partial y} E_x \quad (3).$$

There is likewise a force produced in the y-direction, which is not desirable as it is perpendicular to the length of the channel. Ideally the magnitude of F_x is much greater than that of F_y, and the fluid will reach the outlet of the channel before extensive particle buildup occurs on one of the channel walls (Figure 2).

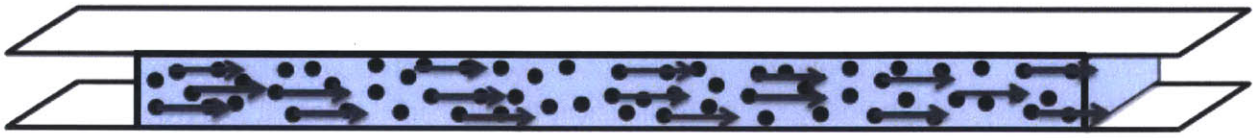

Figure 2: In this model, individual particles each experience a force from the dipole moment generated by electrodes on the channel walls. This force, represented by the grey arrows, pulls on the particles in the direction of the electric field gradient. Particles entrain flow as a result of the drag force from moving through the fluid[15].

One element that has been missing from these studies is the observation of more complex dynamic behavior in the electric fields. The Qian et al. experiments used stepwise increasing potentials to generate their electric fields, but an asymmetric field is required to drive net fluid flow, as detailed in section 2.1.3. The Power Electronics Research Laboratory at Utah State University has been developing a means of creating a moving electric field across a channel. Using a high voltage power supply feeding voltage into a microcontroller, and distributing the voltage to a number of discrete electrodes along the length of a fluid channel, a wider variety of voltages can be produced as a function of both space (i.e. the length of the fluid channel) and time (i.e. periodically changing the voltage at a specific electrode).

These experiments described in this paper address several unknowns associated with this proposed method of pumping. For example, discrete electrodes require physical gaps in between them to function independently, but the behavior of the fluid adjacent to these small gaps has not been well-studied. Additionally, the paper examines the effectiveness of using lower voltages (i.e. hundreds of volts). These questions, along with an analysis of the induced flow, were answered through a combination of computer simulations and physical experiments described below.

Section 2: Predicting and Producing the Flow

Designing a solid-state pump can be broken into two portions- calculations to determine the ideal distribution of voltage along a given set of electrodes, and measurement of flow in an actual channel. The voltage calculations in this paper were generated by a MATLAB simulation

developed by Theresa Hoberg at MIT, and the flow analysis is done through the PIVLab software developed by William Thielicke and Dr. Eize J. Stamhuis at the University of Applied Sciences Bremen.

2.1 MATLAB Simulation

2.1.1. Calculating the Dipole Force

Using equation 3 as a driving principle, Hoberg developed a MATLAB simulation that predicts the force fields in a fluid as a function of channel geometry and input voltages. Calculations are done in a 2D space, which is divided up into a grid of discrete pixels. Electrode voltages for the top and bottom of the channel can either be supplied as functions of length or as discrete values in a matrix. The goal of the MATLAB simulation is to predict which waveforms would produce the greatest net force in the x-direction, in addition to testing waveforms that would produce no net force in the y-direction.

The force calculation is generated by two separate central difference quotient approximations. First, the electric field E_x and E_y at a given pixel is calculated from the definition of an electric field

$$E = -\nabla V, \tag{4}$$

and then the dipole forces F_x and F_y are calculated by taking the gradient of that same electric field as shown in equation 3. Boundary conditions assumed that edge pixels have the same slope as the point adjacent to them. Boundary conditions assumed that the value of an edge pixel was zero. Notably, the MATLAB code does not take into account any losses associated with fluid viscosity or pressure drop along the channel's length. The dipole constant was assumed to be $3 * 10^{-11}$ coulomb-meters, which is the product of the approximate distance between particles and their polarizibility. This is a numerical constant only affecting the magnitude of the output, and not the overall trends of the force field. Rather, the latter is more sensitive to the selection of an appropriate voltage field.

2.1.2. Interpreting the Simulation Output

For these inputs, graphs of the voltage, electric fields, and force fields were generated. The magnitude of a given parameter was indicated with color, creating an overall picture of what force a particle would experience in steady-state flow. The physical experiment does consider time-dependent behavior, elaborated on in Section 2.2.2.

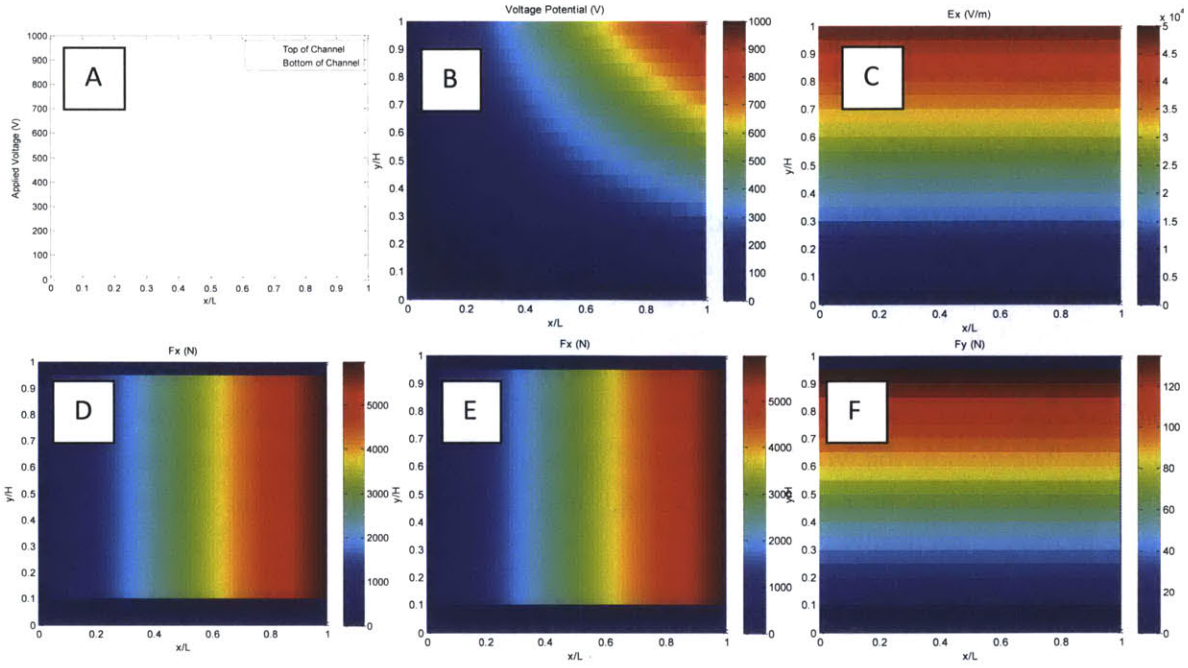

Figure 3: An example of the six graphs generated by Hoberg's simulation. Graph A represents the input voltage waveform, in this example a stepwise linear increase. Graph B respresents how the voltage potential is distributed across a channel. Graphs C and D are the electric field gradients in x and y, respectively. Graphs E and F are the force fields in x and y, respectively. The scales are dimensionless ratios of position to full length. It is worth noting that the x length scale is significantly longer than the y length scale in this example, but because the simulation requires a square field of pixels, the pixel density in the y dimension is greater than that in the x dimension.

2.1.3. Preliminary Results

Several different waveforms were tested using this simulation. As briefly mentioned above, the magnitudes of the forces and fields generated may not be precisely representative of actual values because of the estimated dipole constant, but what are important are the relative magnitudes of the value in one pixel compared to its neighbors. The first simulation shown represents seven electrodes linearly increasing in value.

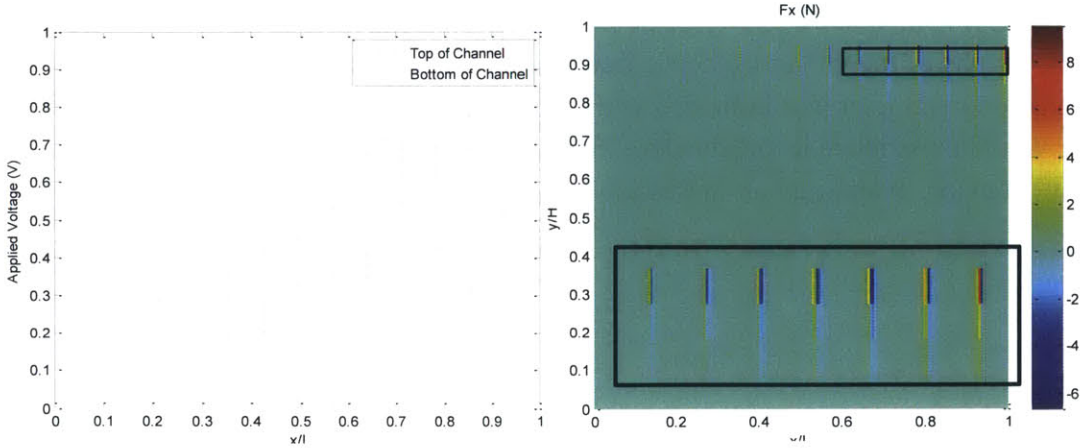

Figure 4: Graphs generated from a linear stepwise voltage input V = x/L. The upper graph shows the voltages applied to the channel walls in a simulation, which in this example are seven distinct electrodes. The lower graph shows the resulting force field for this input, with the net areas of force occurring on the edges of where a physical electrode would be located. The insert is a close-up section of the boxed area in the lower graph, showing that regions of net negative force (dark blue areas) were immediately followed by regions of positive force (red areas).

A preliminary look at the where force was being generated in the simulation suggested that the areas of interest were on the edges of where the physical electrodes would be located, and that a positive force gradient was immediately adjacent to a negative force gradient equal in magnitude. This would cause particles to oscillate in these areas, trapped by the force gradients. To verify the data the forces were summed for a single row of pixels. This summation yielded a net positive force, which was surprising because the values for the electric field strength at the boundaries of the channel are zero. Since dipole force is a conservative field proportional to the gradient of the electric field- which equals zero when the boundary values are zero- then the net value of the force field must also equal zero. It is likely that the fault in this simulation is a result of inaccurate edge conditions and round-off error.

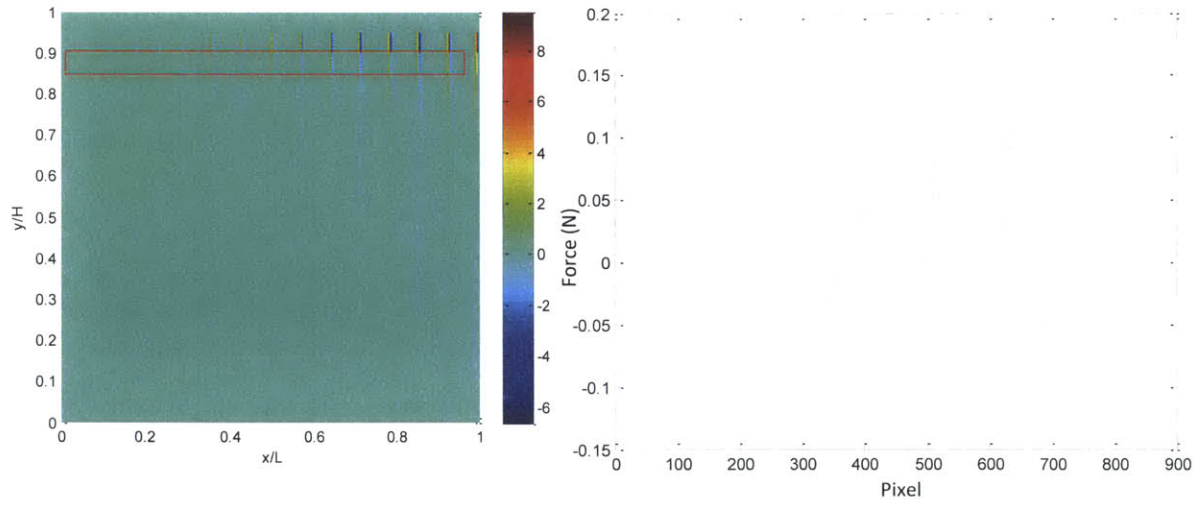

Figure 5: To measure the simulated net force, the values from a single row of pixels, which has been boxed in the graph on the left. On the right, the values of each of the 800 pixels in that row are shown, and the graph was integrated to calculate the net force. There was a net force of 1.02N generated.

2.2 Microscope Slide Experiments

The technology to couple a sophisticated voltage waveform generator to numerous discrete electrodes along a microfluidic channel is currently in the development stage. However, an area of interest (i.e. the spaces between electrodes) can still be observed by placing only two electrodes along a channel.

2.2.1. Pump Design

A solid-state pump consists of three basic components- the fluid channel, electrodes perpendicular to the channel, and the fluid itself. Although traditional quantitative flow measurement is done with a flow meter, for these experiments a video camera and PIVLab were used to estimate flow rates. The electric field gradient required to induce fluid flow is achieved by placing two electrodes next to each other on one side of the channel and a single, larger electrode on the opposite side of the channel. The potential difference is achieved by grounding electrodes on one side of the channel and varying the electrode voltages on the other side of the channel.

A simple channel was constructed for these experiments by sandwiching slides, leaving a gap for the fluid to flow through. Conductive copper tape strips 0.75mm wide were wrapped around the slides to act as electrodes, and their exposed ends were soldered to extension wires that connected to a larger circuit including power supply. The adjacent strips themselves were spaced 0.75mm apart to emulate the equal spacing of the MATLAB simulation electrodes. The channel width was 1.0mm and the height was 1.0mm, or the thickness of a microscope slide. This type of channel can then be placed under a microscope which has sufficient magnification to make the suspended particles visible.

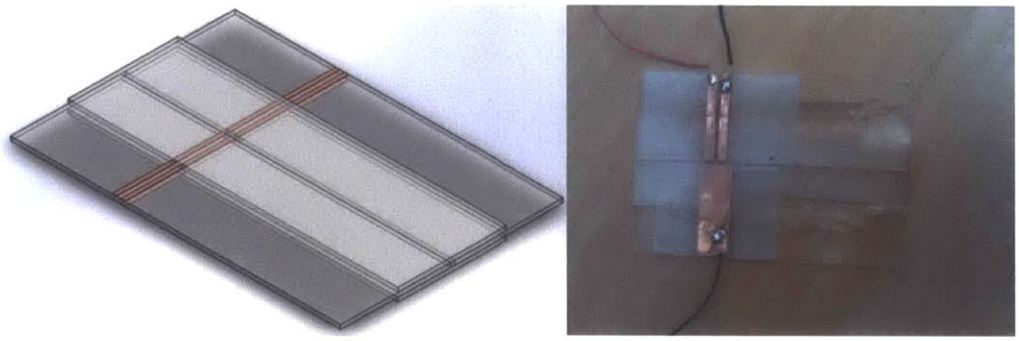

Figure 6: On the left is a Solidworks model of a microfluidic channel. Two scope slides forming the sides of the channel were wrapped in conductive copper tape that was soldered to an external circuit. The top and bottom of the channel were made by sandwiching the two slides that had conductive tape and epoxying the slides together. The gap in the center of the channel is filled with ER fluid, and the behavior between the electrodes can be observed by placing the channel on a microscope. The physical model is on the right, notably with a single ground electrode opposite the two switchable electrodes. Clear tape was wrapped on the edges of the electrodes to prevent leakage of the fluid from the channel. The epoxy was carefully applied as to not block the center channel.

2.2.2. Powering the Pump

A high-voltage (>1 kV) Stanford Research Systems power supply was used to generate the voltage potentials for the channel. The singular electrode on one of the microscope slides was wired to ground. The two electrodes opposing that grounded electrode were wired to a switching circuit that supplied a high voltage to one electrode and ground to the other electrode. The purpose of this switching circuit is to introduce time-dependent situations that are not represented in the MATLAB simulation, specifically, the transition from higher potential near

one end of the channel to higher potential near the opposite end of the channel. The channel itself, after being pre-loaded with ER fluid, is placed on a microscope with 2X magnification.

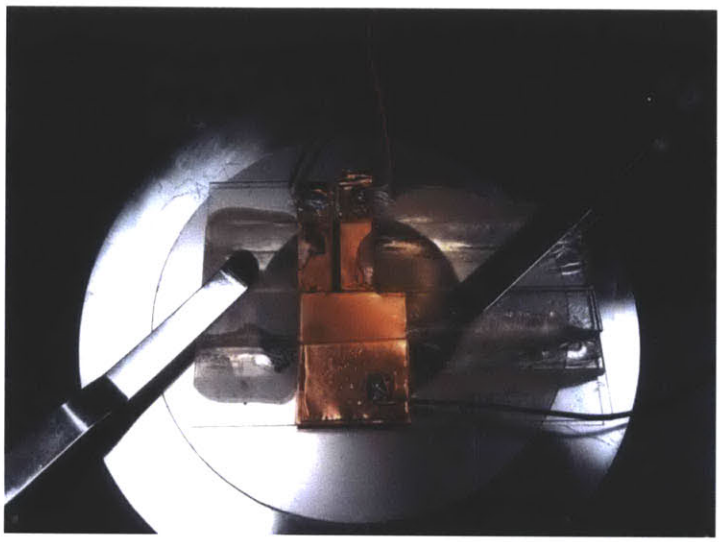

Figure 7: The slide is placed on the microscope, which is connected to an external camera and computer for video collection. Appropriate settings were achieved through a combination of manipulating physical parameters such as light and focal length, and the video parameters of gain and exposure time.

2.2.3. Data Capturing

In these experiments, flow was measured using particle image velocimetry (PIV), a computational technique which allows the user to import a sequence of images of fluid flow. Suspended particles, such as those in the ER fluid used here, are assumed to be representative of the flow. Therefore the spheres in the ER fluid serve a dual purpose in this experiment of both inducing and tracking the flow.

A BlueFOX camera positioned underneath the microscope was connected to the StreamPix program via USB. This program recorded videos, which were then parsed into a series of consecutive images produced from the frames (note that the frame rate varied from experiment to experiment as a result of adjusting the exposure rate to appropriately modify the microscope lighting). Once the images are imported into PIVlab, the user can choose to draw masks selectively around areas where there is not any flow to decrease computational errors and decrease time spent running the software.

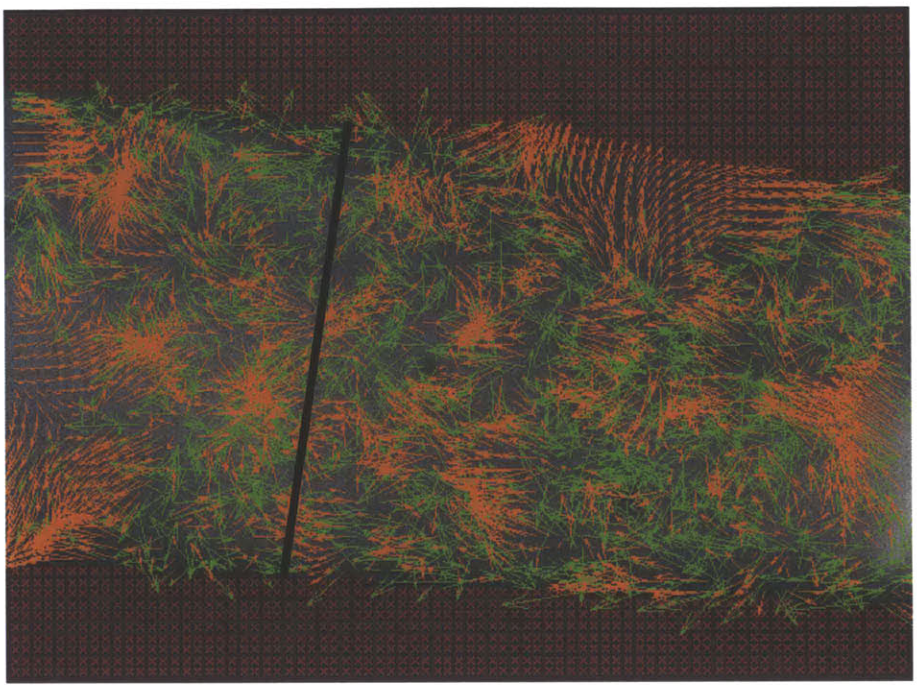

Figure 8: A screenshot from a series of images analyzed using PIVlab. The dark red areas have been masked to avoid erroneous calculations in areas where flow is not occurring, i.e. the walls of the channel. The flow is represented by the colored vectors, with green arrows showing calculated flow and orange arrows showing interpolated flow. Data can be collected from this analysis by drawing a border around the area of interest and specifying the desired parameter, such as velocity. Scale bar is 1mm.

The analysis itself occurs between "frames," which are two sequential images, and the resulting information is displayed as colored vectors. These vectors can be used to derive additional information about the flow field either by drawing a border around a particular area or applying calculations to the entire screen. The user can also manually calibrate the image sequence to convert velocity information from pixels/frame to meters/second.

2.2.4. Analytical Assumptions

Two major assumptions were made while using this software which concern all of the data analysis below. First, because the aim of the experiments was to obtain largely qualitative data about the magnitude and direction of fluid flow, post-processing was applied through a standard deviation filter. This filter eliminates vectors which fall n- standard deviations or further away from the mean, and for these experiments n was set equal to one. Although this tended to eliminate a large number of vectors that appeared in the original calculations, the resulting data provided a clearer image of the general motion of flow in response to the electric field, without compromising the relative magnitudes and directions of the vectors.

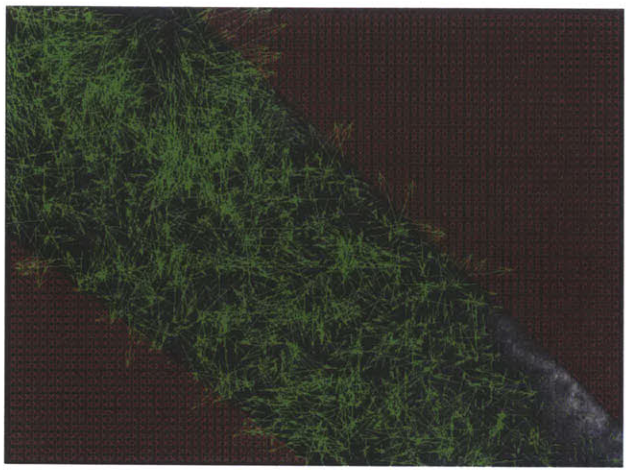

Figure 9: For the raw data produced by PIVlab, the resulting vectors are within an n = 8 standard deviation of the average magnitude vector calculated. It is difficult to interpret where there are areas with net flow due to the volume of vectors produced, which graphically overlap with each other.

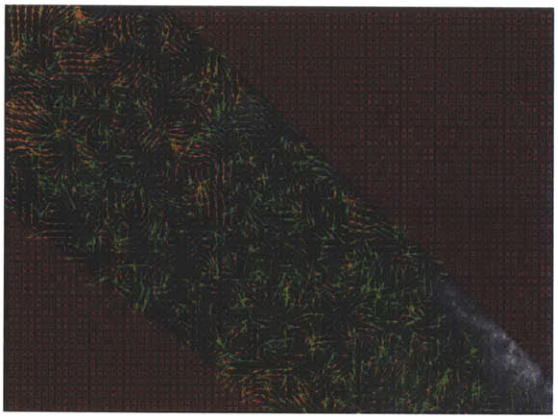

Figure 10: This is the same image sequence that was investigated above, now with vectors within an n = 1 standard deviation. Distinct patterns of flow can be located and isolated for further analysis. One notable detriment of applying a much tighter filter to the vector field is that the magnitudes of the vectors are attenuated, and the calculated net flow rates are therefore lower than what occurred the actual experiment.

The second assumption is that flow velocity is uniform throughout the depth of the channel. Magnification of the channel was low, and the entire image displayed on screen is ideally in focus. Therefore, the image displayed on screen is representative of the fluid at every depth level of the channel, and any PIV analysis has already taken into account any boundary behaviors. Since PIVlab is strictly two dimensional, this assumption allows the calculated flow velocity to be converted to flow rate by multiplying by the depth of the channel.

Section 3: Microscopy Experiments

Each experiment followed the same procedure, with applied voltage as the variable element. First, the channel was filled with ER fluid using a pipette and placed onto the microscope stage. Once on the stage, voltage was applied such that there was a positive electric field gradient from

right to left (Figure 12, left). Video using the BlueFox camera began immediately after the switch was flipped (Figure 12, right), reversing the electric field gradient, and continued for four seconds beyond that time. There were two types of behavior that these experiments aimed to capture: a "gushing" behavior immediately after the switch marked by sudden, high flow rates, and a "steady-state" behavior occurring after that point with a more constant but non-zero flow rate. Frame-by-frame video analysis was able to approximate when the transition between the two states occurred.

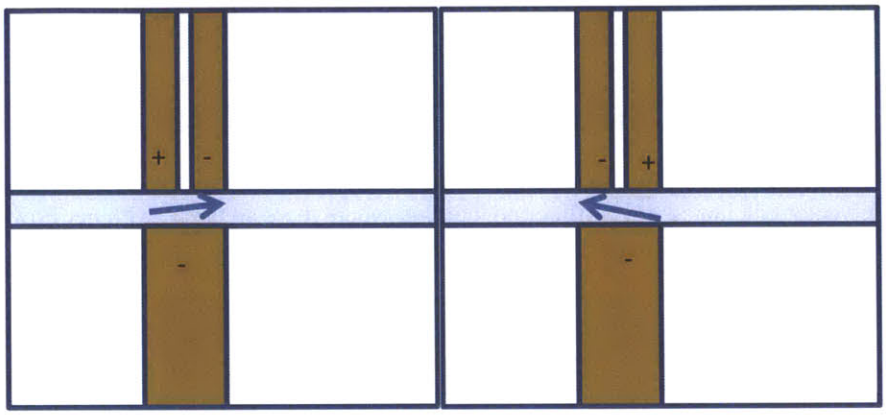

Figure 11: The left side image shows the state of the channel prior to the switch flipping. The arrow represents the gradient of the electric field, as well as the direction of flow, which both of which have a horizontal and vertical component. The right side image is the state after the switch is flipped, which reverses the gradient of the electric field by reversing the voltages on the two upper electrodes. This switch initiates a "gushing" effect with increased fluid flow before settling down again to steady-state flow.

Experimentation began at 1000V, which was the lowest voltage used in the experiments by Qian et al.[17], with lower voltages used in subsequent experiments. Three trials were run at 1000V and at 500V- this was to establish that there was a consistent difference in flow rate that varied with the voltage applied. To determine what was the lowest possible voltage required to yield flow, single trials were run at 300V, 200V, and 100V.

Section 4: PIVLab Analysis

4.1 Identifying the Transition from Gushing Flow to Steady-State

A sudden increase in fluid flow was qualitatively apparent in the videos even without the aid of PIV software, but PIVLab was necessary in quantifying flow rates and determining where an initial peak in velocity ended and a period of steady flow began. An analysis period of four seconds was chosen after examination of longer videos (on the order of tens of seconds) suggested that the flow did not seem to decrease and remained at steady-state values. Each four second period was composed of 210 frames. PIVLab calculated the magnitude of the net velocity in each frame by averaging all of the vectors in that frame.

These 210 frames were grouped into sequential collections of ten frames for the purpose of averaging the net velocities. This yielded 21 average velocities, each of which represented 0.19 seconds of footage. In eight of the eleven experiments, the average velocity appeared to stabilize 0.76 seconds after the switching of voltages, and was thus chosen as the breakpoint between gushing behavior and steady-state for all experimental data collected. This stabilization was indicated by the delta of average velocities from one collection of ten to another decreasing by an order of magnitude.

4.2 History-Dependent Behavior

The experiment was run at 1000V, 500V, 300V, 200V, and 100V to determine the correlation between voltage and flow rate. Several of these experiments yielded a strong history dependence: the flow rate of the ER fluid depends on how it has been introduced to the channel. Before each experiment where a different voltage was supplied, new ER fluid was pipetted into the channel. These experiments are labeled as using "fresh" ER fluid. Subsequent trials at the same voltage reused the same fluid from the previous trial, and are thus labeled as "reused" ER fluid. The effect of replacing the fluid was not apparent when the videos were reviewed by eye but was revealed when the videos were analyzed using PIVLab software.

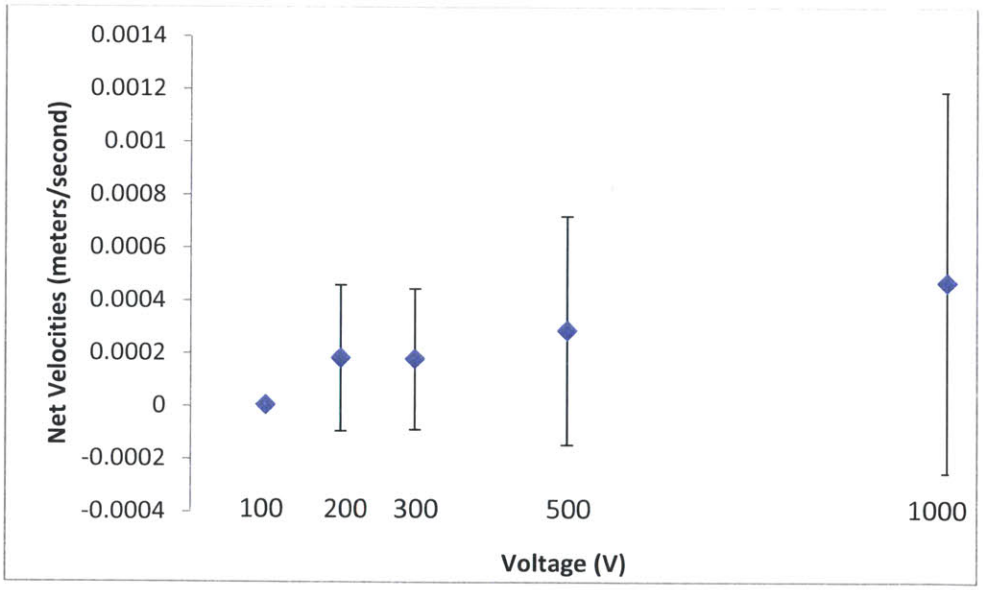

Figure 12: This graph compares applied voltage to net average velocity as calculated in PIVLab for experiments with fresh ER fluid. The data here are from the "gush flow" phase (0.76 seconds following the voltage switch) which corresponds to the highest velocities- and therefore highest flow rates. The average velocities for these experiments were on the order of 10^{-4} m/s. The data used in the remaining sections of the paper was taken from experiments which did not use fresh ER fluid. Error bars indicate the 95% confidence interval.

The first trial for each of the voltages with "fresh" ER fluid yielded average velocities on the order of 10^{-4} m/s, which was an order of magnitude higher than subsequent trials with "reused" ER fluid. One noticeable exception was at 100V, which had the lowest magnitude velocity of

any experiment, which suggests that this may represent a cutoff voltage below which the fluid flow resulting from the induced dipole was not measurable with the given equipment.. This increase in velocity was not entirely clear, and the data from the first trial of any of the voltages were not considered in the remaining analyses in this paper.

4.3 Voltage-Dependent Behavior

Since one of the largest motivations for using a dipole force solid-state pump is that it can operate at lower voltages, it was imperative to determine if the magnitude of the voltage changed the magnitude of the induced flow rate. As noted above, PIVLab-determined velocity dropped off significantly between 200V and 100V. For the experiments used to study voltage-flow rate behavior, three experiments at 1000V and three experiments at 500V were run using "reused" ER fluid. These voltages were selected with the expectation that 1000V would drive the highest flow rates, and 500V would yield a lower but non-zero flow rate. The experiments confirmed these results, with all average flow rates from 1000V experiments exceeding the average flow rates from 500V experiments. The highest flow rate from the 1000V experiments was 175.6 ± 54 mm^3/s and the highest flow rate from the 500V experiments was 15.5 ± 9.6 mm^3/s.

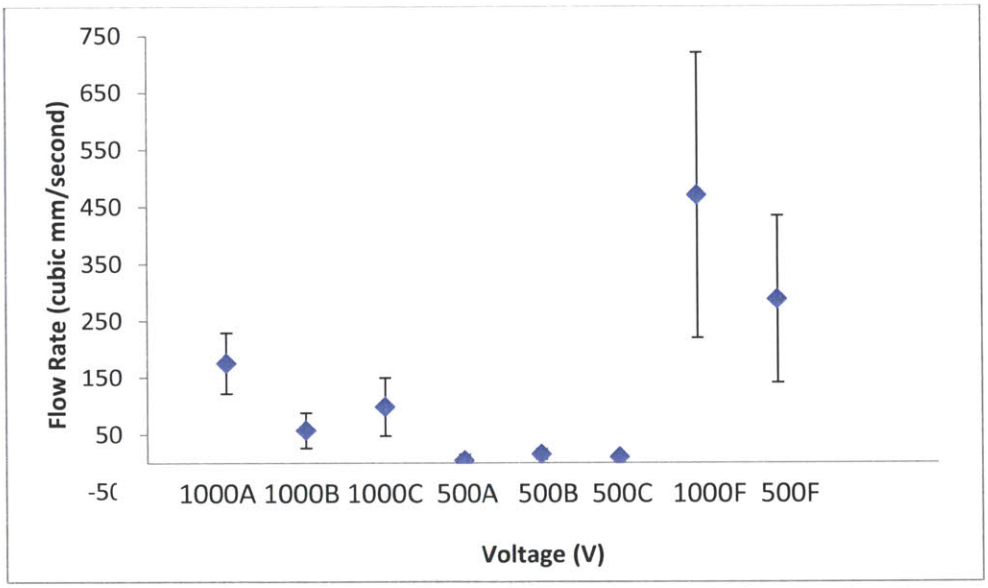

Figure 13: This graph compares the magnitudes of flow rate as a function of applied voltage. The analyzed data came from the "gush flow" phase: 0.76 seconds after switching the voltage. The first six data points were collected with "reused" ER fluid, and the final two for comparison use "fresh" ER fluid. The magnitudes of the 1000V systems were consistently higher than the 500V systems, with all flow rates exceeding $50mm^3/s$. By comparison, the largest 500V flow rate was $15.5mm^3/s$. The error bars indicate the 95% confidence interval.

4.4 Time-Dependent Behavior

As previously mentioned, there appeared to be a distinct difference in flow rates depending on whether the flow occurred right after the voltages were switched or if the flow had already been in motion for several seconds. PIVLab was useful in separating these into two categories of flow-

gush and steady-state. The initial demarcation between the two was calculated by manually determining when the change in velocity from frame to frame decreased by an order of magnitude from the delta that first occurred after the switch, be that from 10^{-4} to 10^{-5} m/s or from 10^{-5} to 10^{-6} m/s. This time scale was found to be 0.76 s in eight of the eleven experiments conducted here. The analysis required after this point was a direct comparison of gush flow rates to steady-state flow rates, which supported the naked eye observation that the gush flow rate was significantly higher.

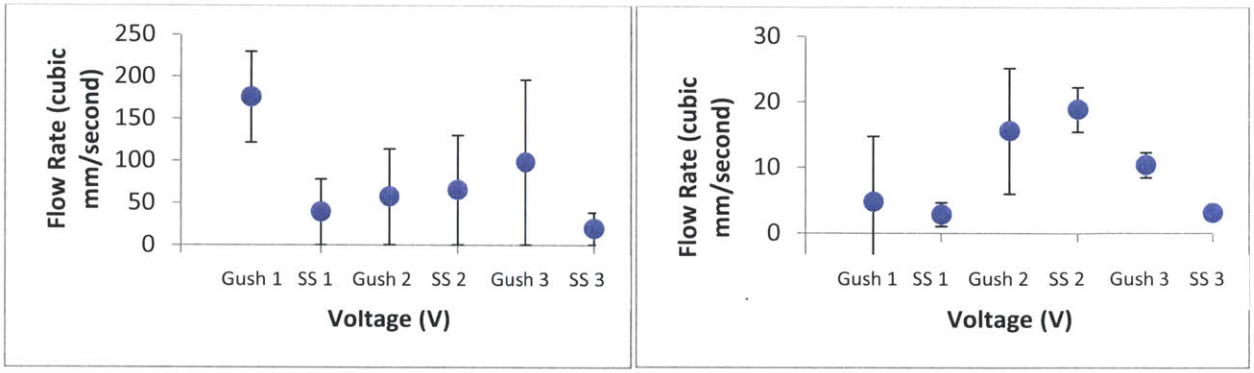

Figure 14: The left graph compares flow rates calculated immediately after the voltage was switched next to flow rates several seconds into steady-state flow for the 1000V experiments. The right graph does the same comparison for the 500V experiments. In both of the graphs, two of the three experiments show noticeably higher flow rates during the gush period, with the third experiment indicating comparable levels of flow. The error bars indicate the 95% confidence interval. SS is an abbreviation for steady-state.

Section 5: Correlation of Simulation and Experimental Data

In general, the MATLAB force calculation simulation was faithful to the experimental data in gross terms of direction and was less reliable in determining magnitude or temporally-dependent situations. At the lowest level, the MATLAB simulation and experimental data agreed that the flow responded to an electric field gradient and occurred in the same direction as the gradient. This correlation was most obvious when observing the channel prior to switching, when the gradient was right to left, and then switched from left to right. The flow clearly transitioned from moving in a direction consistent with the old gradient to a direction consistent to the new gradient, confirming that application of a voltage field varying with time produces net fluid flow in a solid-state pump.

One significant area in which the simulation was helpful was in predicting the presence of flow in both the x- and y- directions, with the x-component parallel to the channel and the y-component perpendicular. In a simulation of linearly increasing force (see Fig. 4) the net forces in x and y were of the same order of magnitude. PIVLab flow calculations produce vectors with a magnitude and angle from horizontal, which allows these vectors to be decomposed into their x and y components. The majority of experiments yielded similar orders of magnitude for both components. This is not ideal for efficient pumping, where the x-component should be

maximized and the y-component minimized. Therefore, in order to design an efficient solid-state pump, electrodes should be placed in such a way to minimize the y-component. This could be achieved, for example, by applying voltages with symmetry in the y-direction.

	X-component (cubic mm/second)	Y-component (cubic mm/second)
1000A	10.3	7.8
1000B	14.3	28
1000C	2.6	21.9
500A	2	0.2
500B	9.8	3.1
500C	1.3	5.2
1000F	220	195
500F	110	114

Figure 15 The values above are the extracted x- and y- components from the steady-state flow experiments at 1000V and 500V. PIVLab generated field vectors with a magnitude and direction, which yielded flow that was neither fully parallel to the channel nor entirely perpendicular to it, with the x- direction being parallel and y- perpendicular. The green color indicates values which were less than one order of magnitude apart. The yellow color indicates a value which was over one order of magnitude larger than its partnered component, and the red color indicates a value which was over one order of magnitude smaller than its partnered component. The majority of the experiments yielded similar orders of magnitude.

As predicted in Section 2.1, the magnitude of the MATLAB simulated dipole forces and the magnitude of the drag forces from the experimental data did not correlate closely. For an input voltage of 1kV, the simulation output a force on a particle of 1kN. For Re << 1, as was the case with this channel, inertial forces were negligible and the fluid drag force should equal the dipole force on a particle. The equation for drag force F_D is

$$F_D = \frac{1}{2}\rho v^2 C_D A, \tag{5}$$

where ρ is the density of the fluid (0.96 kg/L for the silicon oil fluid), v is the particle velocity (the largest observed value was 10^{-3} m/s), C_D is the drag coefficient and A is the surface area of the particle. The silicon oil fluid density is 0.96 kg/L, the fastest observed fluid particle moved at 10^{-3}, and the drag coefficient of a sphere is 0.47. The resulting drag force on this particle is 1.77e-21N, which is significantly lower than the estimated value. This suggests that the estimated dipole constant used in the simulation needs to be recalculated if the drag force from this experiment is valid.

Section 6: Future Work

These experiments helped expand the potential of using solid-state pumps by first showing that net flow is achievable with voltages lower than 1kV and second demonstrating time-dependent behavior at the initial application of voltage that produces flow an order of magnitude higher than steady-state operating conditions. It also produced a number of questions about the nature of solid-state pumps that will require future work to fully understand. Certainly one of the most exciting options on the forefront for these solid-state pumps is a voltage field with a larger number of discrete electrodes and the ability to change the values of voltage applied to a single electrode with time. Dr. Matthew Demers and Dr. Michael Evzelman have been developing the most efficient function of voltage and the circuit to supply that voltage, and there is great potential to produce much higher volumes of fluid flow.

One area that this experiment did not explore was long-term behavior of the pump, mainly because the capacity of the channel constructed from the microscope slides was not large enough to contain the requisite fluid volume. Fluid flow was observed for as long as forty seconds after the initial application of voltage, but the upper limit of this time was not explored. Future research is required to determine if a voltage field could supply indefinite flow capabilities, or if a limiting factor such as particle build-up limits the pump to functioning within a certain timeframe. Answering questions such as these are critical to transitioning these pumps from a laboratory setting to more widespread use.

Bibliography

1. Nelson, G., K. Blanksepoor, and M. Raibert. "Walking BigDog: Insights and Challenges from Legged Robotics." *Journal of Biomechanics* 39 (2006): S360. Print.
2. Murphy, M. P., A. Saunders, C. Moreira, A. A. Rizzi, and M. Raibert. "The LittleDog Robot." *The International Journal of Robotics Research* 30.2 (2011): 145-9. Print.
3. Dimov, Ivan K., Lourdes Basabe-Desmonts, Jose L. Garcia-Cordero, Benjamin M. Ross, Antonio J. Ricco, and Luke P. Lee. "Stand-alone Self-Powered Integrated Microfluidic Blood Analysis System (SIMBAS)." *Lab on a Chip* 11.5 (2011): 845. Print.
4. Purcell, E.M. "Life at Low Reynolds Number." *American Journal of Physics* 45.1 (1977): 3. Print.
5. Purcell, E.M. "Life at Low Reynolds Number." *American Journal of Physics* 45.1 (1977): 3. Print.
6. Yao, Shuhuai, David E. Hertzog, Shulin Zeng, James C. Mikkelsen, and Juan G. Santiago. "Porous Glass Electroosmotic Pumps: Design and Experiments." *Journal of Colloid and Interface Science* 268.1 (2003): 143-53. Print.
7. Winslow, W. M. "Induced Fibration of Suspensions." *Journal of Applied Physics* 20.12 (1949): 1137. Print.
8. Winslow, W. M. "Induced Fibration of Suspensions." *Journal of Applied Physics* 20.12 (1949): 1137. Print.
9. Krieger, Irvin M. "A Mechanism for Non-Newtonian Flow in Suspensions of Rigid Spheres." *Journal of Rheology* 3.1 (1959): 137. Print.
10. Stanway, R. J. L. Sproston, and A. K. El-Wahed. "Appllications of Electro-rheologicl Fluids in Vibration Control: A Survey." *Smart Materials and Structures* 5.4 (1996): 464-82. Print.
11. Liu, Yanju, Rob Davidson, and Paul Taylor. "Touch Sensitive Electrorheolotical Fluid Based Tactile Display." *Smart Materials and Structures* 14.6 (2005): 1563-568. Print.
12. Qian, Bian, Gareth H. McKinley, and A. E. Hosoi. "Structure Evolution in Electrorheological Fluids Flowing through Microchannels." *Soft Matter* 9.10 (2013): 2889. Print.
13. Hoberg, T. "Solid State Pumps for ER/MR Fluid: Design Ideas and Preliminary Analysis." [PDF Document]. Retrieved From https://www.dropbox.com/home/DARPA-actuator/Terri
14. Hoberg, T. "Solid State Pumps for ER/MR Fluid: Design Ideas and Preliminary Analysis." [PDF Document]. Retrieved From https://www.dropbox.com/home/DARPA-actuator/Terri
15. Hoberg, T. "Solid State Pumps for ER/MR Fluid: Design Ideas and Preliminary Analysis." [PDF Document]. Retrieved From https://www.dropbox.com/home/DARPA-actuator/Terri